

Supporting Information

Selective Phase Exposure Induces Ni–Ce Interfacial Redox Reconstruction for CO₂ Activation

Ho-Ryong Park^a, Beom-Jun Kim^a, Su-Jin Ryu^a, Byong-Hun Jeon^b, Hyun-Seog Roh^{a,}*

^a Department of Environmental Engineering, Yonsei University, 1 Yonseidae-gil, Wonju, Gangwon 26493, Republic of Korea

^b Department of Earth Resources and Environmental Engineering, Hanyang University, 222 Wangsimni-ro, Seongdong-gu, Seoul 04763, South Korea

1. EXPERIMENTAL DETAILS

1.1. Catalyst characterization

The in situ XRD analysis was conducted on a SmartLab High Temp (RIGAKU, Japan) with a Cu K α ray source ($\lambda = 0.154$ nm) operating at 45 kV and 200 mA. The catalysts were pre reduced in ex situ condition with 5% H₂/N₂ at 900 °C. The reduced samples were exposed to air with increasing the temperature 7 °C/min from RT to 1000 °C. The patterns were obtained in a 2 θ range from 20 ° to 80 ° at a scan rate of 0.02 °/s. ex situ XRD patterns were collected on a Rigaku Ultima

IV diffractometer with Cu K α radiation (40 kV, 40 mA) in the 2 θ range from 20 ° to 80 ° at a scan rate of 0.02 °/s. For N₂ adsorption–desorption measurements (ASAP 2020, Micromeritics), the samples were degassed at 110 °C for 12 h under vacuum before analysis, and the BET method was applied to determine the specific surface area while the BJH model was used for pore size distribution. High-resolution TEM (JEM-F200, JEOL) was used to investigate the morphology and microstructure of the catalysts. and EDS mapping results of the catalysts were obtained using a FEI Tecnai G2 F20 microscope (ThermoFisher Scientific) at an accelerating voltage of 200 kV. Both as-synthesized and used samples were dispersed in ethanol via ultrasonication and subsequently placed on a copper grid coated with carbon film for TEM analysis. The morphologies of the catalysts were characterized by the field emission scanning electron microscopy (FE-SEM). The dispersion of Ni (D%) was calculated based on the average diameter of Ni nanoparticles obtained from TEM, assuming spherical geometry. The simplified equation is as follows:

$$D(\%) = \frac{6M_{Ni}\sigma}{\rho_{Ni}N_A(D_{diameter} \times 10^{-7})} \times 100\% = \frac{118}{D_{diameter}}(\%)$$

where

M_{Ni} is the molecular weight of Ni (58.69 g mol⁻¹), σ is the areal surface atom density of Ni (1.8 × 10¹⁵ atoms cm⁻²), ρ_{Ni} is the density of Ni (8.908 g cm⁻³), N_A is the Avogadro's number (6.022 × 10²³ mol⁻¹), and $D_{diameter}$ is the mean diameter of Ni nanoparticles (nm) obtained from TEM analysis¹. Based on this calculation, all synthesized catalysts exhibited comparable Ni dispersion values of approximately 12.5%, indicating negligible variation in Ni particle size among the samples. The bulk metal contents were analyzed by ICP-OES (5110 ICP-OES, Agilent). Raman spectra were obtained with a LabRAM Aramis spectrometer (Horiba Jobin Yvon) using a 532 nm laser. H₂-TPR was conducted between 50 and 1000 °C at 10 °C/min, and the reduction degree was

calculated from the integrated H₂ consumption up to 900 °C and 1000 °C according to below equation.

$$\text{Reduction degree (\%)} = \frac{H_2 \text{ consumption amount } (\sim 900 \text{ }^\circ\text{C})}{H_2 \text{ consumption amount } (\sim 1000 \text{ }^\circ\text{C})}$$

XPS spectra were recorded using a K-alpha spectrometer (Thermo Scientific, USA) with an Al K α source, calibrated to the C 1s peak at 284.8 eV. To quantify the OSC, an H₂-O₂ pulse reaction was performed using the Autochem 2920. Before the H₂-O₂ pulse reaction experiment, the catalyst samples were treated with He gas for 2 h, increasing the temperature from 50 °C to 400 °C, followed by exposure to an H₂ pulse using 10 % H₂/Ar at 400 °C to react with mobile oxygen. Subsequently, an O₂ pulse with 10 % O₂/Ar was injected to calculate the OSC based on the amount of O₂ consumed. X-ray absorption fine structure (XAFS) measurements were performed at the 7D XAFS beamline of the Pohang Light Source II (PLS-II), Pohang Accelerator Laboratory (PAL), Republic of Korea. Ni K-edge XAFS spectra were collected in fluorescence mode using a Si(111) double-crystal monochromator. The incident X-ray intensity (I₀) was monitored using an ionization chamber, while the fluorescence signal was detected using a multi-element solid-state detector. Energy calibration was carried out using a Ni metal foil, with the first inflection point of the Ni K-edge set to 8,333 eV. All spectra were recorded at room temperature, and for each sample, three independent scans were collected and averaged to improve the signal-to-noise ratio. In situ and operando DRIFTS measurements were performed using a Nicolet iS50 FT-IR spectrometer (Thermo Scientific, USA) equipped with an MCT detector and a Praying Mantis DRIFTS kit with a high-temperature, standard-pressure reaction chamber (DRK-6-NI8, Harrick Scientific Products, USA). The reaction chamber, made of chemically resistant 316 stainless steel, was equipped with three inlet/outlet ports for gas introduction and evacuation. The catalyst powder was loaded into the sample cup, and the reaction gases were introduced through the chamber under continuous

flow. The spectra were collected at a resolution of 4 cm^{-1} with 16 scans. Prior to the measurements, the catalysts were reduced at $900\text{ }^{\circ}\text{C}$ for 3 h under a 5% H_2/N_2 atmosphere. For in situ CO_2 -DRIFTS, the catalysts were cooled to $50\text{ }^{\circ}\text{C}$ under a continuous N_2 flow, and a background spectrum was collected. The spectra were subsequently recorded in the temperature range of $50\text{--}400\text{ }^{\circ}\text{C}$ under a CO_2 atmosphere while heating at a rate of $10\text{ }^{\circ}\text{C}/\text{min}$. Operando DRIFTS was conducted after the same reduction treatment. The catalysts were heated to $500\text{ }^{\circ}\text{C}$ under a continuous N_2 flow, and a background spectrum was collected at $500\text{ }^{\circ}\text{C}$ before introducing the CH_4/CO_2 feed. The feed gas was then switched to a CH_4/CO_2 mixture (1:3), and the spectra were recorded from 500 to $800\text{ }^{\circ}\text{C}$ with a heating rate of $10\text{ }^{\circ}\text{C}/\text{min}$. To minimize high-temperature thermal-background effects, all spectra were acquired using the same optical alignment, chamber configuration, gas-flow conditions, and temperature-ramping protocol. Because thermal emission and blackbody radiation can reduce the signal-to-noise ratio at elevated temperature, especially near $800\text{ }^{\circ}\text{C}$, the operando DRIFTS spectra were interpreted mainly based on reproducible band evolution and relative differences among catalysts rather than absolute quantitative comparisons of band intensities. Thermogravimetric analysis (TGA) was performed to evaluate carbon deposition on the used catalysts after the SCDR reaction. The used catalysts were recovered after 15 h of reaction and dried prior to analysis. TGA measurements were conducted under an oxidative atmosphere by heating the samples from 50 to $1000\text{ }^{\circ}\text{C}$ at a ramping rate of $10\text{ }^{\circ}\text{C min}^{-1}$. The weight loss observed during heating was used to assess the amount of deposited carbon.

1.2. Activity and stability tests

Catalytic reactions were carried out in a fixed-bed quartz tubular reactor with an inner diameter of 4 mm under atmospheric pressure. The reactor temperature was monitored by a thermocouple

placed at the center of the catalyst bed and controlled by a temperature controller (ss-TFCB-N-2, Samson Hi-Tech, Korea). The catalyst and SiO₂ diluent (Aldrich) were sieved to 50–100 mesh before use. All catalysts were reduced in situ at 900 °C for 3 h under 5% H₂/N₂ before catalytic evaluation. Activity tests were conducted in the range of 500–800 °C. For each run, 12 mg of catalyst was physically mixed with 50 mg of SiO₂ diluent. The feed gas composition was 20% CH₄, 60% CO₂, and 20% N₂, with N₂ serving as both internal standard and diluent. The total flow rate was adjusted to maintain a gas hourly space velocity (GHSV) of 600,000 h⁻¹. Each temperature point was held for 1 h before analysis. Stability evaluation was carried out at 800 °C for 15 and 100 h under the same feed composition. Each gas flow was controlled by an independent mass flow controller (MFC). The effluent gas from the reactor was cooled and then passed through a moisture trap to remove residual H₂O. The resulting gas was then analyzed on-line using a micro gas chromatograph (INFICON Micro GC Fusion, Switzerland). Conversion and yield were defined as follows:

$$CH_4 \text{ conversion (\%)} = \frac{CH_{4in} - CH_{4out}}{CH_{4in}} \times 100 \quad (2)$$

$$CO_2 \text{ conversion (\%)} = \frac{CO_{2in} - CO_{2out}}{CO_{2in}} \times 100 \quad (3)$$

While X_{in} and X_{out} denote the inlet and outlet quantities of X, respectively.

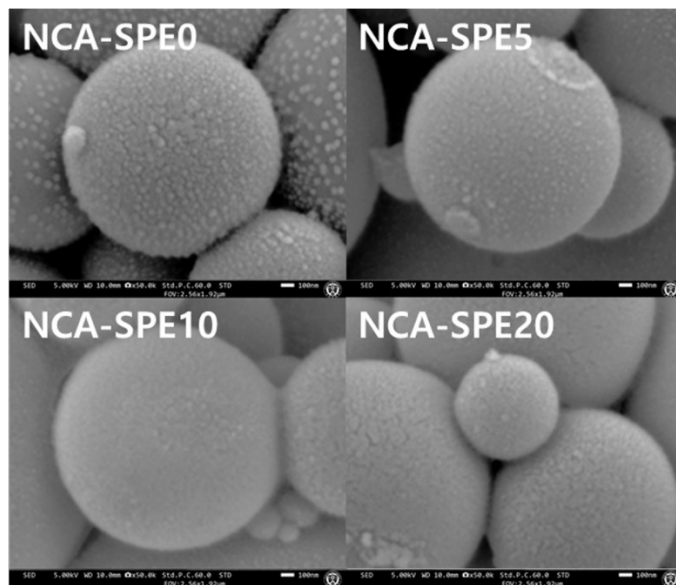


Figure S1. SEM analysis for the as-synthesized NCA-SPE catalysts.

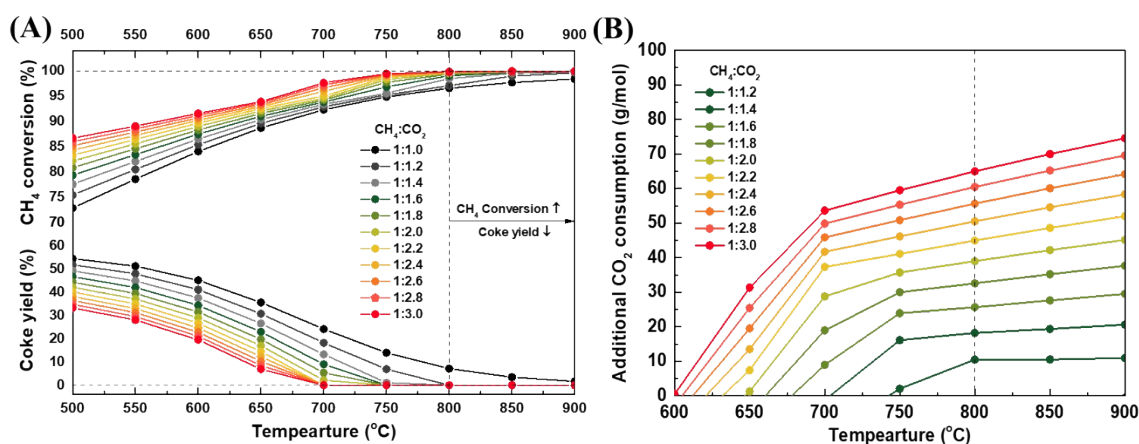


Figure S2. Thermodynamic equilibrium analysis of the SCDR process: (A) CH₄ conversion and carbon yield and (B) additional CO₂ consumption as a function of the CH₄:CO₂ ratio and temperature.

Thermodynamic equilibrium calculations.

Thermodynamic equilibrium calculations were carried out using HSC Chemistry 6.0 based on Gibbs free energy minimization. The system included gas-phase species (CH₄, CO₂, CO, H₂, and H₂O) and solid carbon (C) as a possible product phase. The initial feed composition was set to CH₄:CO₂ = 1:3.

Calculations were performed over a temperature range of 500–900 °C at atmospheric pressure. Equilibrium compositions were obtained assuming ideal gas behavior and complete thermodynamic equilibrium. The temperature-dependent equilibrium compositions were used to evaluate product distribution and the tendency for carbon formation under CO₂-rich reforming conditions.

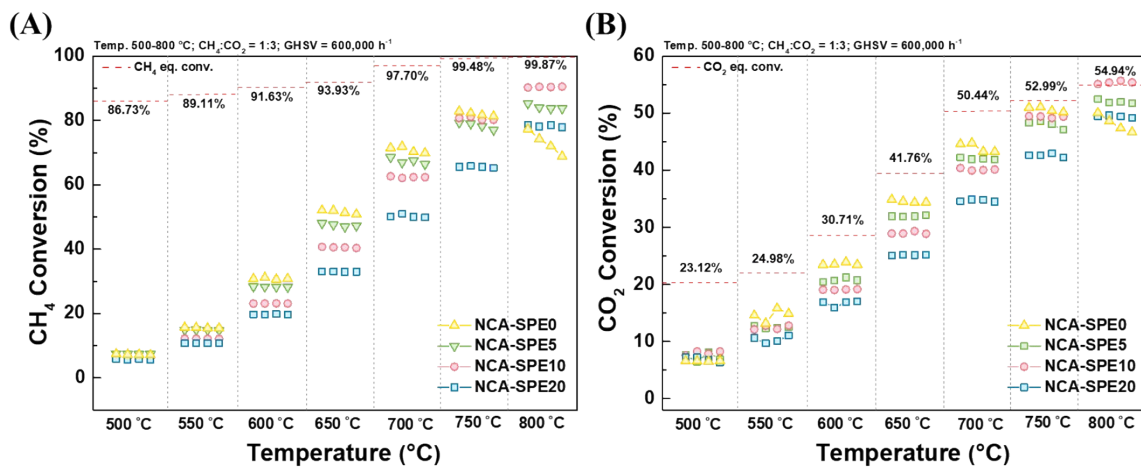


Figure S3. (A) CH₄ and (B) CO₂ conversion at different temperatures (500 – 800 °C).

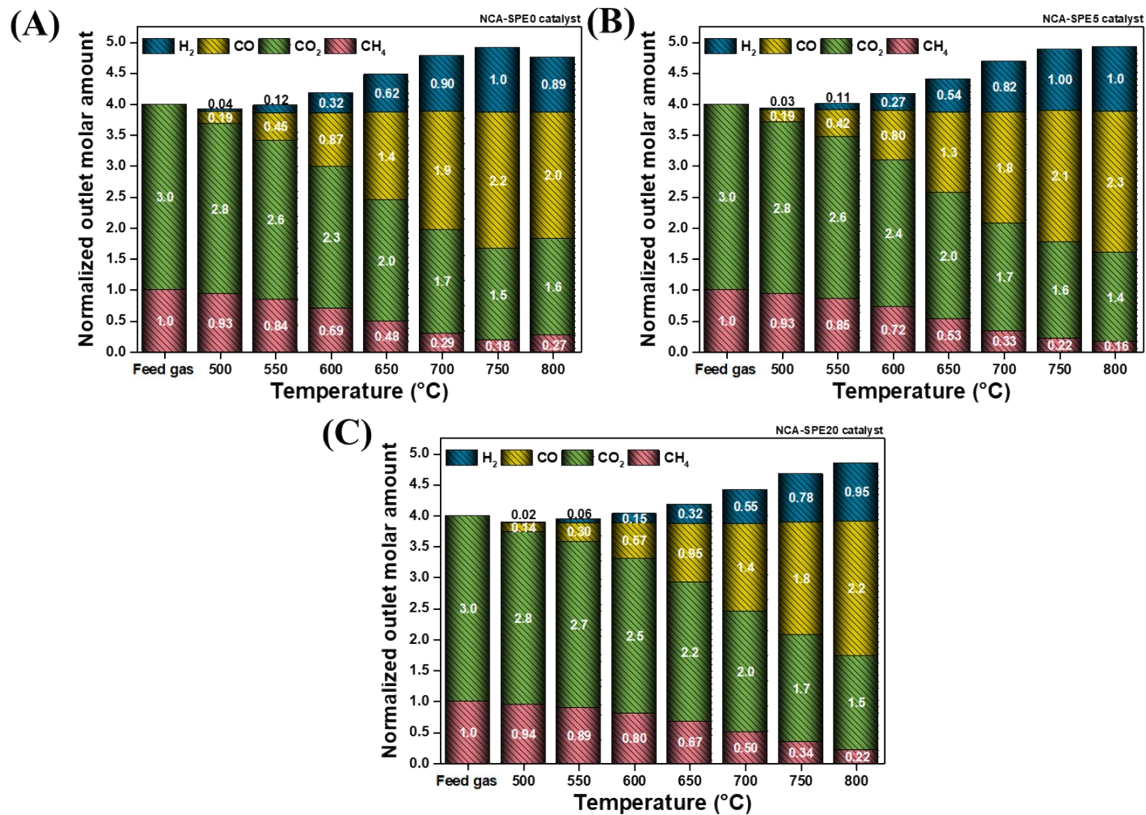


Figure S4. Temperature-dependent product formation over (A) NCA-SPE0, (B) NCA-SPE5, and (C) NCA-SPE20 under CO₂-rich reforming conditions.

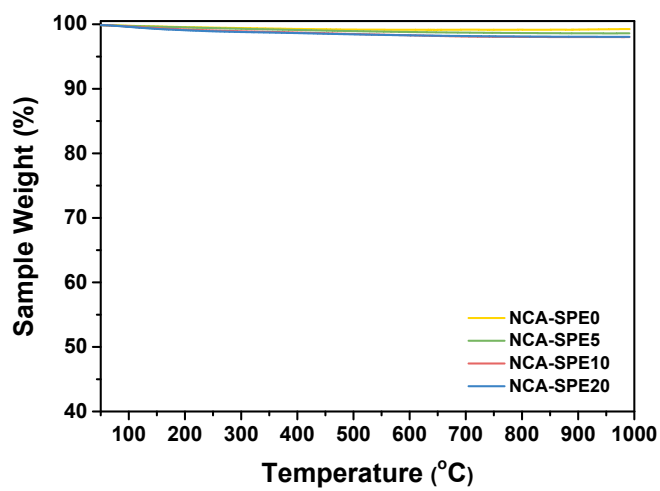


Figure S5. TGA profiles of used NCA-SPE catalysts after SCDR reaction.

REFERENCES

- 1 L. Lin, C. A. Gerlak, C. Liu, J. Llorca, S. Yao, N. Rui, F. Zhang, Z. Liu, S. Zhang, K. Deng, C. B. Murray, J. A. Rodriguez and S. D. Senanayake, *Journal of Energy Chemistry*, 2021, **61**, 602–611.